

UCSF

UC San Francisco Previously Published Works

Title

CRISPR-mediated activation of a promoter or enhancer rescues obesity caused by haploinsufficiency

Permalink

<https://escholarship.org/uc/item/6hx6h7zq>

Journal

Science, 363(6424)

ISSN

0036-8075

Authors

Matharu, Navneet
Rattanasopha, Sawitree
Tamura, Serena
[et al.](#)

Publication Date

2019-01-18

DOI

10.1126/science.aau0629

Peer reviewed



Published in final edited form as:

Science. 2019 January 18; 363(6424): . doi:10.1126/science.aau0629.

CRISPR-mediated activation of a promoter or enhancer rescues obesity caused by haploinsufficiency

Navneet Matharu^{1,2}, Sawitree Rattanasopha^{1,2,3}, Serena Tamura^{1,2}, Lenka Maliskova^{1,2}, Yi Wang⁴, Adelaide Bernard⁴, Aaron Hardin^{1,2}, Walter L. Eckalbar^{1,2}, Christian Vaisse⁴, and Nadav Ahituv^{1,2,*}

¹Department of Bioengineering and Therapeutic Sciences, University of California San Francisco, San Francisco, CA 94158, USA. ²Institute for Human Genetics, University of California San Francisco, San Francisco, CA 94158, USA. ³Doctor of Philosophy Program in Medical Sciences, Faculty of Medicine, Chulalongkorn University, Bangkok, Thailand. ⁴Diabetes Center, University of California San Francisco, San Francisco, CA 94143, USA.

RESEARCH ARTICLE SUMMARY

INTRODUCTION: Loss-of-function mutations in one gene copy can lead to reduced amounts of protein and, consequently, human disease, a condition termed haploinsufficiency. It is currently estimated that more than 660 genes cause human disease as a result of haploinsufficiency. The delivery of extra copies of the gene by way of gene therapy is a promising therapeutic strategy to increase genedosage in such conditions. Recombinant adeno-associated virus (rAAV) provides a promising tool for delivery of transgenes in an efficient and safe way for gene therapy. However, it has some limitations, including an optimal DNA packaging constraint of 4700 base pairs and ectopic expression.

RATIONALE: Increasing the expression levels of the normal gene copy by directly targeting the endogenous gene regulatory elements that control it could potentially correct haploinsufficiency. CRISPR-mediated activation (CRISPRa), whereby a nuclease-deficient Cas9 (dCas9) is used to target a transcriptional activator to the gene's regulatory element (promoter or enhancer), could be used for this purpose. Such an approach could overcome the ectopic expression and DNA packaging limitations of rAAV. Using obesity as a model, we tested in mice whether CRISPR-mediated activation of the existing normal copy of two different genes, *Sim1* or *Mc4r*, where loss-

*Corresponding author. nadav.ahituv@ucsf.edu.

Author contributions: N.M. and N.A. conceived and designed the study. N.M., S.T., and L.M. carried out the cloning and in vitro studies. N.M., S.R., S.T. and A.B. performed the mouse experiments. N.M. and Y.W. carried out the immunostaining, and N.M. performed the stereotactic surgeries and phenotypic analyses. A.H. and W.L.E. helped in making fig. S1. W.L.E. carried out computational analyses of genomic data; N.M., S.R., and N.A. analyzed the data; C.V. and N.A. provided resources and critical suggestions; and N.M. and N.A. wrote the manuscript.

Competing interests: N.A. is an equity holder of, and heads the scientific advisory board for, Encoded Therapeutics, a gene regulation therapeutics company, and N.A. and N.M. are cofounders of Enhancer Therapeutics Inc. N.M. and N.A. are co-inventors on a patent (U.S. Patent US2018017186) submitted by the University of California, San Francisco, that covers gene therapy for haploinsufficiency.

Data and materials availability: All RNA-seq data were deposited in NCBI as Bioproject PRJNA438712. All ChIP-seq data were deposited in NCBI as Bioproject PRJNA438723.

of-function mutations that lead to haploinsufficiency are a major cause of human obesity, can rescue their obesity phenotype.

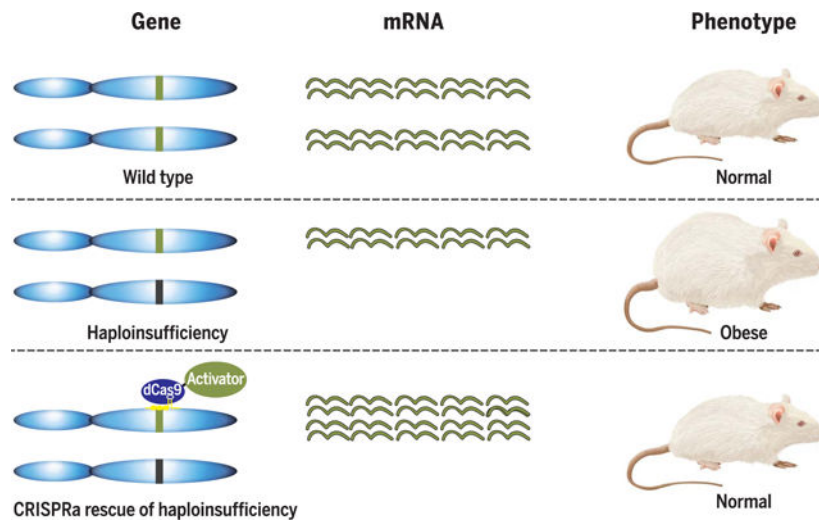
RESULTS: We first generated a transgenic CRISPRa system using dCas9 fused to a transcriptional activator, VP64, to test whether it can rescue the obesity phenotype in a *Sim1* haploinsufficient mouse model. CRISPRa targeting of the *Sim1* promoter or its hypothalamus-specific enhancer, which is 270 kilobases away from the gene, in *Sim1* haploinsufficient mice increased the expression of the normal copy of *Sim1*. This up-regulation was sufficient to rescue the obesity phenotype of *Sim1* heterozygous mice and led to significantly reduced food intake and body fat content in these mice. We assessed the off-targeting effects of CRISPRa using both RNA sequencing (RNA-seq) and Cas9 chromatin immunoprecipitation sequencing (ChIPseq) analyses. We found CRISPRa targeting to be highly specific and without any overt changes in the expression of other genes. We also observed that *Sim1* up-regulation occurred only in tissues where the regulatory element (promoter or enhancer) that was being targeted was active. Although promoter-CRISPRa-targeted mice up-regulated *Sim1* in all the tissues where it is expressed, the enhancer-CRISPRa-targeted mice showed *Sim1* up-regulation only in the hypothalamus. We then delivered CRISPRa packaged into rAAV targeting the *Sim1* promoter or its hypothalamus-specific enhancer using either *Streptococcus pyogenes* or the shorter *Staphylococcus aureus* CRISPRa system. We show that postnatal injection of CRISPRa-rAAV into the hypothalamus can up-regulate *Sim1* expression and rescue the obesity phenotype in *Sim1* haploinsufficient mice in a long-lasting manner. To further highlight the therapeutic potential of this approach to rescue other haploinsufficient genes, we targeted *Mc4r*, where haploinsufficiency leads to severe obesity in mice and humans. CRISPRa-rAAV targeting of the *Mc4r* promoter rescued the obesity phenotype of *Mc4r* heterozygous mice.

CONCLUSION: These findings show that the CRISPRa system can rescue a haploinsufficient phenotype in vivo. This CRISPR-mediated activation strategy is different from a conventional gene therapy strategy, as it uses the endogenous regulatory elements to up-regulate the existing functional gene copy. As such, it can overcome the problem of ectopic gene expression. In addition, it could be used for genes that are not amenable to conventional gene therapy because their coding sequences are longer than the rAAV packaging limit. Our results provide a framework to further develop CRISPRa as a potential tool to treat gene dosage-sensitive diseases.

Abstract

A wide range of human diseases result from haploinsufficiency, where the function of one of the two gene copies is lost. Here, we targeted the remaining functional copy of a haploinsufficient gene using CRISPR-mediated activation (CRISPRa) in *Sim1* and *Mc4r* heterozygous mouse models to rescue their obesity phenotype. Transgenic-based CRISPRa targeting of the *Sim1* promoter or its distant hypothalamic enhancer up-regulated its expression from the endogenous functional allele in a tissue-specific manner, rescuing the obesity phenotype in *Sim1* heterozygous mice. To evaluate the therapeutic potential of CRISPRa, we injected CRISPRa-recombinant adeno-associated virus into the hypothalamus, which led to reversal of the obesity phenotype in *Sim1* and *Mc4r* haploinsufficient mice. Our results suggest that endogenous gene up-regulation could be a potential strategy to treat altered gene dosage diseases.

Graphical Abstract



CRISPRa up-regulation of the existing normal gene copy rescues obesity caused by haploinsufficiency. Loss-of-function mutations in one allele lead to reduced amounts of mRNA and protein and can cause human disease, a condition termed haploinsufficiency. By up-regulating the existing normal allele using CRISPR-mediated activation (CRISPRa), whereby a nuclease-deficient Cas9 is fused to a transcriptional activator and targeted to a gene's regulatory element (promoter or enhancer), the haploinsufficient phenotype could be rescued.

More than 660 genes are currently estimated to cause human disease due to haploinsufficiency (table S1) (1,2), leading to a wide range of phenotypes that include cancer, neurological diseases, developmental disorders, immunological diseases, metabolic disorders, infertility, kidney disease, limb malformations, and many others (1, 2). Large-scale exome sequencing analyses estimate that there could be over 3000 human genes that are haploinsufficient (3). Gene therapy in which a functional recombinant copy or copies replace the mutant gene holds great promise in addressing diseases caused by haploinsufficiency. Numerous clinical trials are being carried out for gene therapy, most of which use recombinant adeno-associated virus (rAAV) to deliver the transgene (4). rAAV is a preferred gene delivery method because of its ability to provide long-lasting gene expression of the transgene, delivering DNA without integrating into the genome, and with limited pathogenicity (5). However, current rAAV approaches tend to use promoters to drive transgenes that can lead to undesirable ectopic expression (6, 7). Another crucial limitation is that AAV has an optimal 4.7-kilobase (kb) packaging capacity (8), limiting its gene therapy use for genes longer than 3.5 kb (taking into account additional regulatory sequences needed for its stable expression). Analysis of the 660 haploinsufficiency disease-causing genes and 3230 predicted heterozygous loss-of-function (LoF) genes reveals that 135 (20%) and 730 (23%) of them, respectively, have coding sequences longer than 3.5 kb (fig. S1), rendering them unsuitable for rAAV gene therapy.

CRISPR gene editing can potentially fix haploinsufficient mutations; however, this would require that the editing strategy be custom-tailored for each mutation. Moreover, it may not be feasible to correct heterozygous LoF microdeletions. To address these challenges, we

devised a strategy that could potentially treat haploinsufficiency by using CRISPR activation (CRISPRa). CRISPRa takes advantage of the RNA-guided targeting ability of CRISPR to direct a nuclease-deficient Cas9 (*dCas9*) fused with a transcriptional activator to regulatory element(s) of a specific gene, thus increasing its expression (9–15). Here, we tested whether this system can be used to rescue a haploinsufficient phenotype by increasing the transcription of the normal endogenous gene. As a proof-of-concept model, we chose a quantitative trait, obesity caused by haploinsufficiency of either the single-minded family basic helix-loop-helix (bHLH) transcription factor 1 (*Sim1*) or the melanocortin 4 receptor (*Mc4r*) gene.

SIM1 is a transcription factor that is expressed in the developing kidney and central nervous system and is essential for the formation of the supraoptic nuclei (SON) and paraventricular nuclei (PVN) of the hypothalamus (16). *SIM1* also plays a role in the maintenance of long-term energy homeostasis by acting downstream of the leptin-melanocortin pathway (17). In humans, haploinsufficiency of *SIM1* due to chromosomal aberrations results in hyperphagic obesity (18), and *SIM1* coding mutations, many of which are LoF mutations, are thought to be a major cause of severe obesity in humans (19–21). *Sim1* homozygous null mice die perinatally, whereas *Sim1* heterozygous mice (*Sim1*^{+/-}) survive, are hyperphagic, and develop early-onset obesity with increased linear growth, hyperinsulinemia, and hyperleptinemia (22). A postnatal conditional knockout of hypothalamic *Sim1* leads to a similar phenotype in heterozygous mice (23), delineating an additional role for *Sim1* as an important regulator of energy homeostasis in adults. Overexpression of *SIM1*, by using a human bacterial artificial chromosome in mice, rescues diet-induced obesity and reduced food intake (24), suggesting a potential role for *SIM1* in preventing development of an obesity phenotype.

MC4R is a heterotrimeric guanine nucleotide-binding protein (G protein)-coupled receptor that is essential for the long-term regulation of energy homeostasis and other physiological processes. MC4R expression in the PVN of the hypothalamus is both necessary and sufficient for most of its effects on the regulation of body weight (25). Heterozygous mutations in *MC4R* are the most common cause of monogenic severe obesity, estimated at 2.6 to 5% of cases of early-onset and/or adult class 3 obesity (body mass index >40 kg/m²) (26–28). Mice haploinsufficient for *Mc4r* become obese with hyperphagia, hyperinsulinemia, and hyperglycemia (29).

We initially tested the ability of a transgenic CRISPRa system to rescue the obesity phenotype in *Sim1*^{+/-} mice. CRISPRa using a single guide RNA (sgRNA) targeted to either the *Sim1* promoter or its ~270-kb distant enhancer up-regulated *Sim1* expression and rescued *Sim1*-mediated obesity in haploinsufficient animals. This transgenic approach also showed that *Sim1* up-regulation occurred only in tissues where the promoter or enhancer is active, suggesting that the targeted cis-regulatory elements can determine CRISPRa tissue specificity. We also used these transgenic mice to assess the targeting specificity of CRISPRa by using RNA sequencing (RNA-seq) and chromatin immunoprecipitation sequencing (ChIP-seq), which we found to be highly specific and without any apparent off-target effects. To further show that CRISPRa could be used as a potential strategy to treat haploinsufficient phenotypes, we used rAAV-mediated delivery of CRISPRa to the

hypothalamus, preventing excessive weight gain in postnatal *Sim1*^{+/-} mice. To demonstrate that this strategy could be used for other haplo-insufficient genes, we also targeted the *Mc4r* promoter by means of a similar CRISPRa-rAAV approach and reduced weight gain in *Mc4r*^{+/-} mice. Our results present a potential strategy for treating haploinsufficiency and additional gene dosage-related functional abnormalities.

Results

Up-regulation of *Sim1* in vitro by CRISPRa

To increase expression of the wild-type *Sim1* gene, we optimized CRISPRa conditions in vitro. *Sim1* has a well-characterized promoter (30) and distant and robust hypothalamic enhancer (~270 kb from the transcription start site) denoted *Sim1* candidate enhancer 2 [SCE2 (31)] (Fig. 1A). To target *Sim1* using CRISPRa, we designed two sgRNAs for either the *Sim1* promoter or SCE2. Using these guides, we tested whether *Streptococcus pyogenes* dCas9 fused to VP64 (spdCas9-VP64), a transcriptional activator that carries four tandem copies of VP16 (a herpes simplex virus type 1 transcription factor) (32), can up-regulate *Sim1* in mouse neuroblastoma cells (Neuro-2a). The VP64 activator domain was chosen primarily because of its small size (so that it could later fit in our rAAV plasmid). It is also known to have a moderate activation potential compared to other known activators for a wide variety of genes (33), which could be advantageous in obtaining physiologically relevant *Sim1* dosage levels in vivo. Cells were transfected with spdCas9-VP64 and the various guide RNAs. After 48 hours, *Sim1* mRNA levels were measured by quantitative polymerase chain reaction (qPCR). We identified one sgRNA for either promoter or SCE2 that could up-regulate endogenous *Sim1* by 13- and 4-fold respectively (Fig. 1B and fig. S2, A and B). We also carried out ChIP-seq using an antibody against *S. pyogenes* Cas9 in both CRISPRa-promoter- and CRISPRa-enhancer-transfected cells and found on-target binding for the promoter and enhancer, respectively (fig. S2, C and D). We did not observe any peaks that overlapped with predicted sgRNA off-targets (table S2).

Up-regulation of *Sim1* in vivo by transgenic CRISPRa rescues obesity

To test the ability of the CRISPRa system to rescue obesity in *Sim1*^{+/-} mice, we generated knockin mouse lines using TARGATT technology (34). Using this technology, we inserted *spdCas9-VP64* into the mouse *Hipp11* locus [a region that is known to allow robust transgene expression (35)] having three copies of attP (*H11P3*^{CAG-dCas9-VP64}) and either sgRNA, targeting the *Sim1* promoter (*R26P3*^{Sim1Pr-sgRNA}) or SCE2 (*R26P3*^{SCE2En-sgRNA}), in the *Rosa26* locus that has three attP sites (Fig. 1C and fig. S3). We then crossed these mice to *Sim1*^{+/-} mice that develop severe obesity (22). Mice having all three alleles (*Sim1*^{+/-} × *H11P3*^{CAG-dCas9-VP64} and *R26P3*^{Sim1Pr-sgRNA} or *R26P3*^{SCE2En-sgRNA}) were weighed weekly until 16 weeks of age along with wild-type littermates and *Sim1*^{+/-} and *Sim1*^{+/-} × *H11P3*^{CAG-dCas9-VP64} mice, both of which become severely obese (negative controls). Analysis of at least 10 females and 10 males per condition showed that *Sim1*^{+/-} mice carrying both spdCas9-VP64 and either *Sim1* promoter or enhancer sgRNA had a significant reduction in body weight compared to *Sim1*^{+/-} × *H11P3*^{CAG-dCas9-VP64} and *Sim1*^{+/-} (Fig. 1, D and E, and fig. S4). *Sim1*^{+/+} mice carrying *spdCas9-VP64* and either *Sim1* promoter or enhancer sgRNA also showed a reduction in body weight compared to

wild-type mice (fig. S4). We also analyzed body fat content and food intake for all genotypes: *Sim1*^{+/-} × H11P3^{CAG-dCas9-VP64} × R26P3^{Sim1Pr-sgRNA} (*Prm*-CRISPRa), *Sim1*^{+/-} × H11P3^{CAG-dCas9-VP64} × R26P3^{SCE2En-sgRNA} (*Enh*-CRISPRa), *Sim1*^{+/-}, and wild-type mice. Both *Prm*-CRISPRa and *Enh*-CRISPRa mice showed significantly reduced body fat content and food intake compared to *Sim1*^{+/-} in both females and males (fig. S5). Of note, we observed slight differences in body weight trajectories between female and male mice (i.e., when compared to wild-type mice, *Sim1*^{+/-} females gained weight more rapidly than males), similar to what was observed in previous *Sim1* knockout studies (22,23). Taken together, these results show that both *Prm*-CRISPRa and *Enh*-CRISPRa mice have reduced body weight due to lower food intake, which likely leads to their reduced body fat levels.

CRISPRa up-regulation of *Sim1* is tissue specific

To test for *Sim1* activation levels and tissue specificity in *Prm*-CRISPRa and *Enh*-CRISPRa mice, we measured its mRNA expression levels in different tissues. We selected two tissues where *Sim1* is expressed, hypothalamus and kidney, and two tissues where it is not expressed, lung and liver, based on previous studies (36,37) and our analysis of *Sim1* expression in different tissues (fig. S6). We first measured *spdCas9* expression and found it to be expressed in all four tissues, as expected, because we used a ubiquitous cytomegalovirus (CMV) enhancer chicken β-actin (CAG) promoter to drive its expression (Fig. 2A). By contrast, for *Sim1*, we observed significantly higher mRNA levels in both the hypothalamus and kidney in *Prm*-CRISPRa mice but only in the hypothalamus of *Enh*-CRISPRa mice compared to *Sim1*^{+/-} mice (Fig. 2B). In *Sim1*^{+/-} mice, we observed half the levels of mRNA expression when compared to wild-type mice, both in the hypothalamus and kidney.

Because we did not observe any significant differences between the obesity phenotype of *Prm*-CRISPRa and *Enh*-CRISPRa mice, we speculate that the activation of *Sim1* in the hypothalamus is sufficient to rescue the *Sim1*^{+/-} obesity phenotype. In tissues where *Sim1* is not expressed (i.e., liver and lung), we could not detect *Sim1* expression in *Prm*-CRISPRa or *Enh*-CRISPRa mice despite *spdCas9* being expressed. These results imply that despite ubiquitous expression, *spdCas9-VP64* could only up-regulate *Sim1* in tissues where its target cis-regulatory elements are active. This suggests that cis-regulatory elements could be used to define the tissue specificity of CRISPRa.

Sim1 CRISPRa targeting is highly specific

To check for CRISPRa off-target effects, we undertook two genomic-level approaches: We analyzed the hypothalamic transcriptome (RNA-seq) of wild-type, *Sim1*^{+/-}, *Prm*-CRISPRa, and *Enh*-CRISPRa mice. Three males and three females were used for each genotype (total of 24 samples; 6 biological replicates per condition). We also carried out ChIP-seq using an antibody against *S. pyogenes* Cas9 in the hypothalamus of *Prm*-CRISPRa, *Enh*-CRISPRa, and *spdCas9-VP64* (negative control) mice. A pool of four mice was used for each genotype, and two biological replicates.

In the RNA-seq analyses, we identified 24 differentially expressed genes [at a false discovery rate (FDR) of 0.1] between *Sim1*^{+/-} and wild-type mice, of which 17 were up-

regulated and 7 were down-regulated. For all of the 17 up-regulated and 6 of the 7 down-regulated genes, we observed fold changes that were similar to that of wild-type versus *Sim1*^{+/-} for Prm-CRISPRa or Enh-CRISPRa when compared to *Sim1*^{+/-} (Fig. 2, C and D, and table S3). We also observed that genes that were significantly up-regulated or down-regulated in Prm-CRISPRa versus *Sim1*^{+/-} were also up-regulated or down-regulated in Enh-CRISPRa and vice versa, highlighting that the overall gene expression profile in Prm-CRISPRa and Enh-CRISPRa was similar (Fig. 2, C and D, and table S3). None of the *Sim1* neighboring genes within a 500-kb window were differentially expressed in Prm-CRISPRa or Enh-CRISPRa in the RNA-seq analysis. Using qPCR, we also analyzed the mRNA expression levels of *Sim1* neighboring genes, activating signal cointegrator 1 complex subunit 3 (*Ascc3*) and G protein-coupled receptor class C group 6 member A (*Gprc6a*). We did not observe any differences in expression levels for these genes in Prm-CRISPRa and Enh-CRISPRa compared to wild-type mice (fig. S7, A and B). These results suggest that *Sim1*-CRISPRa changes the transcription profile of *Sim1*^{+/-} mice to one that is more similar to that of the wild type.

Next, we carried out ChIP-seq analysis to identify off-target *spdCas9*-VP64 binding. We found the most significant on-target enrichment at the *Sim1* promoter in Prm-CRISPRa and SCE2 in Enh-CRISPRa mice (fig. S8, A and B, and table S2). In addition, we found 91 and 136 significant peaks (FDR adjusted *p* value = 10⁻¹) in Prm-CRISPRa and Enh-CRISPRa, respectively (table S2). We then looked for predicted sequence-specific genomic off-targets due to Prm-sgRNA or Enh-sgRNA mismatches, allowing for zero to three nucleotide mismatches, using Cas-OFFfinder (38). For the promoter-targeting sgRNA, we found the one expected on-target site, and one off-target site with three nucleotide mismatches (fig. S8C and table S2). For the enhancer-targeting sgRNA, we found the one expected on-target site and eight off-target sites with three nucleotide mismatches (fig. S8D and table S2). None of the Prm-CRISPRa or Enh-CRISPRa ChIP-seq peaks overlapped a corresponding predicted off-target site (table S2).

We next analyzed the RNA-seq datasets for the expression of the neighboring genes (\pm 500 kb upstream and downstream) near the ChIP-seq peaks and sgRNA off-target sites, including the *Sim1* target-specific peaks (fig. S8, C and D, and table S3). Of the genes within 500 kb of the off-target ChIP-seq peaks or predicted off-target sites, none showed differential gene expression (Fig. 2, E and F, and fig. S8, E and F). In addition, ChIP for dCas9 followed by qPCR for *Ascc3*, *Gprc6a*, and the *Sim1* promoter or SCE2 showed binding only in the *Sim1* promoter for Prm-CRISPRa and SCE2 in Enh-CRISPRa mice (fig. S7, C and D), similar to what we observed in the ChIP-seq data. Our results show that *Sim1* Prm-CRISPRa and Enh-CRISPRa are highly specific, without any apparent off-target effects.

Delivery of *Sim1* CRISPRa rAAV to the PVN rescues the weight gain phenotype in *Sim1*^{+/-} mice

To further investigate the translational potential of this approach to rescue haploinsufficiency in adult mice, we took advantage of rAAV to deliver CRISPRa into the hypothalamus of *Sim1*^{+/-} mice. We generated the following three rAAV vectors: (i) *S. pyogenes* dCas9-VP64 driven by a CMV promoter (*pCMV-spdCas9-VP64*); (ii) *Sim1* promoter sgRNA along with

mCherry (*pU6-Sim1Pr-CMV-mCherry*); and (iii) SCE2 sgRNA along with mCherry (*pU6-SCE2-CMV-mCherry*) (Fig. 3A). These vectors were packaged individually into AAV-DJ serotype (39). We first tested if the rAAV CRISPRa vectors could up-regulate *Sim1* in vitro using Neuro-2a cells. We observed a four- and fivefold increase in *Sim1* mRNA expression when targeting the promoter or enhancer, respectively (Fig. 3B and fig. S9).

Next, we performed stereotactic injections to deliver virus carrying *pCMV-spdCas9-VP64* and either *pU6-Sim1Pr-CMV-mCherry* (Prm-CRISPRa-AAV) or *pU6-SCE2-CMV-mCherry* (Enh-CRISPRa-AAV) into the PVN of the hypothalamus of *Sim1^{+/-}* mice at 4 weeks of age, before the mice start becoming obese. As an injection-based negative control, we also injected *Sim1^{+/-}* mice with *pCMV-spdCas9-VP64* virus only. We first optimized the stereotaxic injection conditions and coordinates (see Methods) and tested for the expression of mCherry from the *pU6-Sim1Pr-CMV-mCherry* cassette in the PVN by performing immunostaining on the hypothalami of injected mice (Fig. 3C and fig. S10). Next, we carried out stereotaxic injections into the PVN of *Sim1^{+/-}* mice at 4 weeks of age using *S. pyogenes* CRISPRa-AAV. To test whether *Sim1* expression levels were increased by delivering CRISPRa-AAV to the hypothalamus of *Sim1^{+/-}* mice, we measured mRNA expression levels for both *dCas9* and *Sim1* from 11-week-old AAV-injected mice. *dCas9* was expressed in the hypothalami of all the *pCMV-spdCas9-VP64* AAV-injected mice (Fig. 3D). *Sim1* up-regulation was observed in both Prm-CRISPRa-AAV- and Enh-CRISPRa-AAV-injected hypothalami, but not in mice injected with only *pCMV-spdCas9-VP64*-AAV (Fig. 3E). To observe the extent of *Sim1* up-regulation that could be achieved, we injected Prm-CRISPRa-AAV into the hypothalami of wild-type mice using two different titers. We observed up to 1.8-fold up-regulation with the higher viral titer (fig. S11).

Because the length of *S. pyogenes* dCas9-VP64 exceeds the optimal packaging load for AAV (i.e., 4.7 kb), we generated a *Staphylococcus aureus* dCas9-fused VP64 vector, which has an AAV packaging load of 4.3 kb (Fig. 3A; *pCMV-sadCas9-VP64*). As *S. aureus* uses a different protospacer adjacent motif site, we designed and cloned sgRNAs for *pU6-Sim1Pr-CMV-mCherry* and *pU6-SCE2-CMV-mCherry*. We identified several sgRNAs that can increase *Sim1* expression by targeting its promoter or SCE2 in Neuro-2a cells through transient transfection (fig. S12, A and B). We also carried out ChIP-seq using an antibody against *S. aureus* Cas9 in both Prm-CRISPRa- and Enh-CRISPRa-transfected cells and found on-target binding for the promoter and enhancer, respectively (fig. S12, C and D). We did not observe any peaks that overlapped with predicted sgRNA off-targets (table S2). We then generated an AAV-DJ serotype of the *S. aureus* CRISPRa vectors, obtaining higher titers for dCas9-VP64 virions than *S. pyogenes* CRISPRa-AAVs (see Methods). We infected Neuro-2a cells with the viruses and selected a single sgRNA for the promoter or SCE2 that significantly increased *Sim1* expression (Fig. 3B and fig. S12E). Next, we carried out stereotactic injections into the PVN of *Sim1^{+/-}* mice at 4 weeks of age using *S. aureus* CRISPRa-AAV. To test whether *Sim1* expression levels were increased by delivering *S. aureus* CRISPRa-AAV to the hypothalamus of *Sim1^{+/-}* mice, we measured mRNA expression levels from hypothalami of 11-week-old AAV-injected mice. Compared to *S. pyogenes* dCas9 expression levels (Fig. 3D), we found higher expression levels of *S. aureus* dCas9 in the hypothalami of all *pCMV-sadCas9-VP64* AAV-injected mice (Fig. 3F). We also observed higher *Sim1* up-regulation (Fig. 3G) compared to *S. pyogenes* CRISPRa (Fig. 3E).

Next, we tested whether *Sim1* up-regulation by CRISPRa-AAV can lead to a reduction in body weight of *Sim1* haploinsufficient mice. CRISPRa-AAV-injected *Sim1*^{+/-} mice were measured for body weight up to 11 weeks of age (Fig. 4A). We observed a significant weight reduction in the Prm-CRISPRa-AAV- or Enh-CRISPRa-AAV- injected mice compared to the *Sim1*^{+/-} or *pCMV-dCas9-VP64-AAV*-injected *Sim1*^{+/-} mice both for *S. pyogenes* (Fig. 4B) and *S. aureus* (Fig. 4C). These results suggest that CRISPRa-AAV can rescue the *Sim1* haploinsufficiency obesity phenotype.

Finally, we analyzed whether CRISPRa would have a long-term body weight effect on these mice. Although many of the injected mice were analyzed in the aforementioned gene expression studies, a few were maintained and showed significant weight reduction compared to the *Sim1*^{+/-} or *pCMV-spdCas9-VP64-AAV*-injected *Sim1*^{+/-} mice 9 months after injection (Fig. 4, D and E). Similar results were also observed in *S. aureus*-injected mice (fig. S13). These results show that CRISPRa-AAV-mediated up-regulation could have a long-lasting effect on phenotype.

Delivery of Mc4r CRISPRa rAAV to the PVN rescues the weight gain phenotype in Mc4r^{+/-} mice

To further investigate whether CRISPRa can rescue an additional haploinsufficient obesity model, we carried out *S. aureus* CRISPRa targeting of the *Mc4r* promoter in *Mc4r*^{+/-} mice, which become obese as a result of heterozygous LoF of *Mc4r* (29). We first screened five sgRNAs targeting the *Mc4r* promoter and selected one that led to robust *Mc4r* up-regulation in Neuro-2a cells using both transient transfection and rAAV infections (fig. S14). We then carried out stereotactic injections into the PVN of 4-week-old *Mc4r*^{+/-} mice with either *pCMV-sadCas9-VP64-AAV* as a negative control or *pCMV-sadCas9-VP64-AAV* and *pU6-Mc4rPr-CMV-mCherry* (*Mc4rPrm-CRISPRa-AAV*) (Fig. 5, A and B). We observed an increase in *Mc4r* expression up to 2.7-fold in *Mc4rPrm-CRISPRa-AAV* mice (Fig. 5C). Body weight measurements 8 weeks after injection showed a significant weight reduction in the *Mc4rPrm-CRISPRa-AAV*-injected mice compared to the *Mc4r*^{+/-} or *pCMV-sadCas9-VP64AAV*-injected *Mc4r*^{+/-} mice (Fig. 5, D and E). These results further suggest that CRISPRa can be used to rescue other haploinsufficient phenotypes.

Discussion

CRISPR-based gene editing is a promising therapeutic technology for correcting genetic mutations. However, it is a challenging approach for treating haploinsufficiency, limited by low homology-directed repair efficiencies (i.e., editing only a small portion of cells) and the need to custom-tailor specific guides and donor sequences for each individual mutation. In addition, it may not be a feasible therapeutic strategy for microdeletions, more than 200 of which are known to cause human disease (40), primarily because of haploinsufficiency. In this study, we used a CRISPR-mediated activation approach to tackle these hurdles and show how a haploinsufficient phenotype could be corrected by increasing the transcriptional output from the existing functional allele with CRISPRa.

Using CRISPRa targeting for either the promoter or enhancer of *Sim1*, we could rescue the obesity phenotype in a tissue-specific manner in mice that are haploinsufficient for *Sim1*.

Because this approach takes advantage of the existing functional allele, it has several benefits: (i) It overcomes the need to custom-tailor CRISPR gene editing approaches for different haploinsufficiency-causing mutations in the same gene. (ii) This approach could potentially be used to target two or more genes. It could serve as a potential therapeutic strategy for microdeletions-related diseases that are caused by the heterozygous LoF of more than one gene. (iii) CRISPRa-AAV could be used to rescue haploinsufficient phenotypes caused by genes that are longer than its optimal packaging capability. (iv) Tissue specificity is a major concern for gene therapy. CRISPRa-based approaches can take advantage of cis-regulatory elements to guide tissue specificity (Fig. 6A). The availability of large-scale tissue-specific maps of gene regulatory elements could provide ample candidates for this approach. We observed distinct differences in tissue-specific activation of *Sim1* based on the targeted cis-regulatory element, which can be attributed to chromatin accessibility of the locus in various tissues. Previous large-scale Cas9 and dCas9 cell culture screens have shown a targeting preference for regions with low nucleosome occupancy (41,42). Active promoters or enhancers would have lower nucleosome occupancy, thus being more amenable to dCas9 targeting.

CRISPRa uses a nuclease-deficient Cas9 (dCas9) fused to a transcriptional activator and as such does not edit the genome. However, it can lead to transcriptional modulated off-target effects. To test for such effects, we carried out both RNA-seq and ChIP-seq in vitro and in vivo. We did not observe any apparent CRISPRa off-target binding that resulted in significant transcriptional changes. Additional analyses of predicted off-targeting loci due to sgRNA mismatches did not find any transcriptional changes surrounding these loci. The dCas9-VP64 fusion used in our CRISPRa system is known to activate loci that are programmed for transcription, such as promoters or enhancers (14,42). Taken together, our results suggest that CRISPRa has high specificity.

Our dCas9-VP64 mouse and rAAV vectors can be a useful tool for targeted gene activation in vivo by delivering sgRNA(s) targeted to a specific gene in certain tissues or cell types. This approach could be used to assess gene-gene interactions or for the identification of the target gene(s) of a specific regulatory element in vivo by measuring its expression level following activation. Another potential area of study could be neuronal circuit manipulation. Discrepancies between acute and chronic neuronal circuit manipulations have been observed (43) that could potentially be addressed by rAAV-CRISPRa and transgenic-CRISPRa strategies, respectively.

Haploinsufficiency of *SIMI* is associated with severe obesity (19–21) in humans and mice (22). Whether this is caused by the reduction in PVN size during development that is observed in *Sim1*^{+/-} mice (22) or by disturbed energy homeostasis during adulthood was largely unknown. The obesity phenotype observed in the postnatal conditional knockout of hypothalamic *Sim1* (23) reinforced the hypothesis that *Sim1* does indeed have a role in energy homeostasis later during adulthood. Our results showing phenotypic rescue in adult mice by rAAV CRISPRa further corroborate this role.

Mutations in *MC4R* are the most commonly found in individuals with class 3 obesity (body mass index >40 kg/m²), with an estimated 2.6 to 5% of this population having mutations in

this gene (26–28). Heterozygous LoF mutations in this gene are associated with an obesity phenotype (26–28). MC4R is a promising drug target for anti-obesity drugs, and several agonists have been developed to target this receptor (44,45). Here, we decreased the weight gain in *Mc4r*^{+/-} mice using rAAV-CRISPRa targeting of the *Mc4r* promoter.

CRISPRa-based gene activation is highly dependent on the nature of the fused activator (33) and sgRNA target (41) and would need to be optimized for a particular gene, along with the delivery method. It is important to note that overexpressing genes beyond their physiologically relevant doses could have undesirable side effects. The use of a shorter dCas9, such as the *S. aureus* (46) that was used in this study, could reduce the packaging load and improve dCas9 delivery, with optimal up-regulation levels to achieve physiologically relevant results. This approach can also lead to increased expression of the mutant allele, if the targeted promoter or enhancer is not deleted, and may not be useful in cases where this allele is not a complete LoF. In addition, targeting rAAV to specific neuronal populations in primates may require multiple injections or other DNA delivery methods.

We demonstrate that CRISPRa can be used to activate genes in vivo not only by targeting their promoters but also by targeting distal cis-regulatory elements such as enhancers. We were able to rescue a haploinsufficient phenotype in a long-lasting manner (9 months) with CRISPRa-rAAV by targeting either the promoter or enhancer of a gene. Previous studies have shown that these elements can be potential therapeutic targets. For example, by targeting a globin enhancer with zinc finger nucleases fused to a chromatin looping factor, the LIM domain binding 1 (*LDB1*) gene, activation of fetal hemoglobin was achieved in vitro, providing a potential therapy for sickle cell disease (47). In another study, reactivation of fetal hemoglobin was achieved by deactivating the enhancer of its repressor B cell CLL/lymphoma 11A (*BCL11A*) using CRISPR gene editing (48). Our study provides an approach in preclinical mouse model systems that takes advantage of cis-regulatory elements and can aid in designing potential therapeutic strategies. Numerous phenotypes caused by lower gene dosage could potentially be targeted with CRISPRa (Fig. 6B). In addition, several human diseases could potentially be rescued by the activation of another gene with a similar function (Fig. 6C). These could include, for example, *Utrophin* for Duchenne muscular dystrophy (DMD) (49, 50), survival of motor neuron 2 (*SMA2*) for spinal muscular atrophy (51), or fetal globin for sickle cell disease. For example, a CRISPR-based approach (CRISPR/Cas9 TGA) was recently shown to ameliorate the dystrophic phenotype upon up-regulation of either the *Utrophin*, *Klotho*, or *Fst* genes in a mouse model of DMD (50). Further development of gene up-regulation by CRISPRa or other techniques could provide a potential therapy for dosage-related diseases.

Materials and methods

Plasmids

The *pMSCV-LTR-dCas9-VP64-BFP* vector, encoding a mammalian codon-optimized *Streptococcus pyogenes* dCas9 fused to two C-terminal SV40 NLSs and tagBFP along with a VP64 domain and the U6-sgRNA-CMV-mCherry-T2A-Puro plasmids were used for cell line transfections (both kind gifts from J. S. Weissman and S. Qi). sgRNAs (table S4) were

cloned using the In-Fusion HD-cloning kit (Clontech) following the manufacturer's protocol into the Bst XI and Xho I sites. Mouse knockin vectors were generated by cloning dCas9-VP64 and U6-sgRNA-CMV-mCherry expression cassettes from the aforementioned vectors into the TARGATT (CAG + Poly A) plasmid (Applied StemCell). For AAV vectors, *pcDNA-dCas9-VP64* (Addgene 47107), and U6-sgRNA-CMV-mCherry-WPREpA were cloned replacing the *Ef1a-FAS-hChr2(H134R)-mCherry-WPRE-pA* with that of the U6-sgRNA-CMV-mCherry-WPREpA into the backbone of *pAAV-Ef1a-FAS-hChr2(H134R)-mCherry-WPRE-pA* (Addgene 37090). *S. aureus* dCas9-VP64 vector was constructed from Addgene Plasmid #68495, AAV-NLS-dSaCas9-NLS-VPR by removing the RelA(p65) activation domain and Rta Activation domain using XbaI and EcoRI enzymes and introducing a stop codon after the VP64 domain followed by bGHPolyA. We named it *pAAV-CMV-sadCas9-VP64-pA*. *pAAV-U6-sasgRNA-CMV-mCherry-WPREpA* was cloned by replacing the *CMV-sadCas9-VP64-pA* cassette in *pAAV-CMV-sadCas9-VP64-pA* backbone with that of *U6-sasgRNA-CMV-mCherry-WPREpA* cassette from *pLTR-1120-MPI77-U6-sasgRNA-mcherry* (a kind gift from B. Huang at UCSF). *S. aureus* sgRNAs (table S4) were cloned using the In-Fusion HD-cloning kit (Clontech) following the manufacturer's protocol into the Bst XI and Xho I restriction enzyme sites.

AAV production

Particles of rAAV-DJ serotype, which is a chimera of type 2,8, and 9 that was shown to achieve high expression levels in multiple tissues (39), were produced for all vectors using the Stanford Gene Vector and Virus core. The packaging load for *pCMV-spdCas9-VP64* was 5.4 kb and for *pU6-Sim1Pr-CMV-mCherry* and *pU6-SCE2-CMV-mCherry* 2.5 kb. Genomic titers were ascertained by WPRE and ITR probes to be 1.40×10^{10} viral genome (vg)/ml for *pCMV-spdCas9-VP64* and around 3.30×10^{13} vg/ml for *pU6-Sim1Pr-CMV-mCherry* and 2.20×10^{13} vg/ml for *pU6-SCE2-CMV-mCherry*. The packaging load for *pCMV-sadCas9-VP64-pA* was 4.3 kb and for *pU6-sasgRNA-CMV-mCherry* was 2.5 kb. Genomic titers for *pAAV-CMV-sadCas9-VP64-pA* were 1.60×10^{12} vg/ml, for *pU6-sasgRNA3Sim1Pr-CMV-mCherry* 1.58×10^{13} vg/ml, for *pU6-sasgRNA3SCE2-CMV-mCherry* 2.0×10^{13} vg/ml, and for *pU6-sasgRNA2Mc4rpr-CMV-mCherry* 1.0×10^{13} vg/ml.

Cell culture

Neuroblastoma 2a cells (Neuro-2a; ATCC[®] CCL-131) were grown following ATCC guidelines. Plasmids were transfected into Neuro-2a cells using X-tremeGENE HP DNA transfection reagent (Roche) following the manufacturer's protocol. AAV particles were infected into Neuro-2a cells at different multiplicity of infection (MOI) ratios (figs. S9 and S12E). Neuro-2a cells were harvested 48 hours after transfection and 5 days after infection to isolate RNA for qRT-PCR analysis.

RNA isolation, RNA-seq, and quantitative reverse-transcription PCR

RNA was isolated from cells or tissues using RNeasy Mini Kit (Qiagen) following the manufacturer's protocol. For mice, animals were euthanized and tissues were harvested directly into the RNA lysis buffer of the RNeasy Mini Kit. The hypothalamus was dissected using a mouse brain matrix and slicers (Zivic Instruments). Each hypothalamus was sampled the same way for each animal with 1.0-mm coronal section slice intervals. The coronal brain

section of the hypothalamus was sliced with two blades 3 mm apart (fig. S15, A to C). The hypothalamus was dissected out from this coronal section. Care was taken to orient the brain on the matrix and to align the hypothalamus each time corresponding to the same coronal section slots. For qRT-PCR, cDNA was prepared using SuperScript III First-Strand Synthesis System (Invitrogen) using the manufacturer's protocol along with deoxyribonuclease I digestion. qPCR was performed with SsoFast EvaGreen Supermix (Bio-Rad) using the primers indicated in table S4. To further validate our qPCR results for *Sim1*, we also performed qPCR on wild-type, *Sim1^{+/-}* and *Sim1^{+/-}* Prm-CRISPRa-AAV-, Enh-CRISPRa-AAV-, or *pCMV-dCas9-VP64-AAV-injected* mice with primers that overlap the region that was knocked out (*Sim1-5'* primers listed in table S4), obtaining similar results (fig. S13, D to G). The results were expressed as fold-increase mRNA expression of the gene of interest normalized to either *Actb* or *Rpl38* expression by the $2^{-\Delta\Delta CT}$ method followed by analysis of variance (ANOVA) and Tukey test for statistical analysis. Reported values are the mean \pm SEM from three independent experiments performed on different days ($N=3$) with technical duplicates that were averaged for each experiment. For RNA-seq, three males and three females were used for each genotype (24 samples total; 6 biological replicates per condition). cDNA was amplified using Ovation V2 kit (NuGEN), and sequencing libraries were generated using NexteraXT kit (Illumina). RNA-seq was carried out on an Illumina HiSeq 4000. Sequence alignment was performed using STAR (52). Mappings were restricted to those that were uniquely assigned to the mouse genome and unique read alignments were used to quantify expression and aggregated on a per-gene basis using the Ensembl (GRCm38.67) annotation. Analyses of individual hypothalamus expressed genes (*Agrp*, *Crh*, *Oxt*, *Pomc* and *Trh*) showed a good correlation between individual samples in each condition (fig. S15, D to H). We analyzed these raw data using DESeq2 (53) to assess variance and differential expression between sample groups. All RNA-seq data was deposited in NCBI as Bioproject PRJNA438712.

Chromatin immunoprecipitation

Fresh tissue was homogenized using a hand-held dounce homogenizer, cross-linked in phosphate-buffered saline (PBS) containing 1% formaldehyde for 10 min, quenched with 125 mM glycine for 5 min, and washed three times with PBS. Crosslinked tissue pellet was processed further for chromatin immunoprecipitation using the Low cell Chip Kit (Diagenode; catalog no. C01010072) following the manufacturer's protocol. An *S. pyogenes* Cas9 polyclonal antibody (Diagenode; catalog no. C15310258) and an *S. aureus* Cas9 monoclonal antibody (Diagenode; catalog no. C15200230) were used for the pull-down. Enrichment of target regions were assessed by RT-qPCR using SsoFast EvaGreen Supermix (Bio-Rad) and primers listed in table S4. Results were expressed as %input using the $2^{-\Delta\Delta CT}$ method. Reported values are the mean \pm SEM from three independent experiments performed on different days ($N=2$) with technical duplicates that were averaged for each experiment. For ChIP-seq, a pool of four mice was used for each genotype and two biological replicates. Libraries were made by using the ThruPLEX DNA-seq kit (Rubicon Genomics; catalog no. R400428) and sequencing was carried out with an Illumina HiSeq-4000. Sequencing reads were mapped to the genome using STAR (52). Mapping was restricted to reads that were uniquely assigned to the mouse genome (GRCm38.67). Replicates were pooled to call peaks against a background of the nontargeting VP64 ChIP

using MACS2 (54). All CHIP-seq data were deposited in NCBI as Bioproject PRJNA438723.

Mice

Sim1^{+/-} mice (22) on a mixed genetic background were obtained as a kind gift from J. Michaud's lab. In these mice, a 1-kb fragment containing 750 bp of the 5' region, the initiation codon, and the sequence coding for the basic domain (the first 17 amino acids) was replaced by a *Pgk-neo* cassette that was used for genotyping (see table S4 for primers) with KAPA mouse genotyping kit (KAPA Biosystems). To generate dCas9-VP64 and sgRNA mice, we used TARGATT technology (34). DNA for injection was prepared and purified as minicircles by using the TARGATT Transgenic Kit, V6 (Applied StemCell). The injection mix contained 3 ng/μl DNA and 48 ng/μl of in vitro-transcribed ϕC31o mRNA in microinjection TE buffer [0.1 mM EDTA, 10 mM Tris (pH 7.5)], and injections were done using standard mouse transgenic protocols (55). dCas9-VP64 was inserted into the mouse *Hipp11* locus and sgRNAs into the *Rosa26* locus. Mice were genotyped using the KAPA mouse genotyping kit. F₀ H11P33 TARGATT knockins were assessed using PCR primers SH176 + SH178 + PR432 and for ROSA26 primers ROSA10 + ROSA11 + PR432 described in (34) along with vector insertion-specific dCas9-VP64 primers as well as mCherry-specific primers (described in table S4). *Mc4r*^{+/-} mice on C57BL/6 background were genotyped using MC4R1, MC4F3, and PGKR3 primers (table S4). In these mice, a deletion of 1.5 kb starting from 20 nucleotides downstream of the *Mc4r* initiation codon to ~500 bp after 3' of the gene was replaced by a *Pgk-neo* cassette (29). All mice were fed ad libitum Picolab mouse diet 20,5058 containing 20% protein, 9% fat, 4% fiber for the whole study. Calories were provided by protein (23.210%), fat (ether extract) (21.559%), and carbohydrates 55.231%. All animal work was approved by the UCSF Institutional Animal Care and Use Committee.

Transgenic mice body weight measurements

HHP3^{CAG-dCas9-VP64} *R26F3*^{sim1Pr-sgRNA} and *R26P3*^{SCE2En-sgRNA} mice were mated with *FVB* mice for three to five generations to assess germ-line transmission. Three independent integrants were used from each line to set up matings. *H11P3*^{CAG-dCas9-VP64} were mated with *Sim1*^{+/-} and subsequent *Sim1*^{+/-} × *H11P3*^{CAG-dCas9-VP64} mice were crossed with either *R26F3*^{Sim1Pr-sgRNA} or *R26P3*^{SCE2En-sgRNA} to generate mice having all three unlinked alleles. Mice were maintained at Picodiet 5058 throughout the study, and at least 10 females and 10 males from all genotypes (wild type, *Sim1*^{+/-}, *Sim1*^{+/-} × *H11Ps*^{CAG-dCas9-VP64}, *Sim1*^{+/-} × *H11Ps*^F^{CAG-dCas9-VP64} × *R26P3*^{Sim1Pr-sgRNA}, *Sim1*^{+/-} × *H11F3*^{CAG-dCas9-VP64} × *R26F3*^{SCE2En-sgRNA}) were measured for their body weights from 4 to 16 weeks of age on a weekly basis.

Body composition and food intake analyses

Body composition was measured using either dual energy x-ray absorptiometry (DEXA) or Echo Magnetic Resonance Imaging (EchoMRI; Echo Medical System). For DEXA, mice were anesthetized with isoflurane and measured for bone mineral density and tissue composition (fat mass and lean mass) with the Lunar PIXImus. EchoMRI (Echo Medical System) was used to measure whole-body composition parameters such as total body fat,

lean mass, body fluids, and total body water in live mice without the need for anesthesia or sedation. Food intake was measured by using the Columbus Instruments Comprehensive Lab Animal Monitoring System (CLAMS; Columbus Instruments). Mice were housed individually and acclimatized on powdered picodiet 5058 for 3 to 4 days, and food intake measurements were done over 4 to 5 days. Three males and three females from each genotype: wild-type littermates, *Sim1*^{+/-}, *Sim1*^{+/-} × *H11P3*^{CAG-dCas9-VP64} × *R26P3*^{Sim1Pr-sgRNA}, *Sim1*^{+/-} × *H11P3*^{CAG-dCas9-VF64} × *R26P3*^{SCE2En-sgRNA} were measured.

Stereotaxic injections

Four-week-old *Sim1*^{+/-} or *Mc4r*^{+/-} males or females, weighing between 20 and 26 g were housed individually in cages for at least 2 days before surgical interventions. Mice were anesthetized with 3% isoflurane for induction and 1% isoflurane for maintenance in a vaporizer chamber. The skull was immobilized in a stereotaxic apparatus (Model 1900, Stereotaxic Alignment Systems, 1micron resolution, David Kopf Instruments). The stereotaxic coordinates for injection into the PVN were 0.80 mm caudal to bregma, 0 mm at the midline, and 5.2 mm below the surface of the skull, similar to the midline injections carried out in a previous study (56). A 0.5-mm hole was created in the cranium with a high-speed model 1911 Stereotaxic Drill with a 0.02-inch drill bit (David Kopf Instruments). Using a 31-gauge 1- μ l Hamilton microsyringe, we injected a dose of 0.5×10^7 vg/ml of sgRNA-AAV along with 2.5×10^6 vg/kg of spdCas9-VP64-AAV or 0.8×10^7 vg/ml of sadCas9-VP64-AAV in a total injection volume of 1 μ l per animal into the PVN unilaterally over a 10-min period. This titer and double the amount (1×10^7 vg/ml of sgRNA-AAV along with 5×10^6 vg/ml of spdCas9-VP64-AAV) were also injected into 5-week-old wild-type FVB mice (fig. S11). After rAAV delivery, the needle was left in place for 20 min to prevent reflux and slowly withdrawn in several steps, over 10 min. Mice were administered two doses of buprenorphine (100 mg/kg) before and 24 hours after surgery. Mice were only excluded from the study for the following reasons (table S6): (i) having shorter bregma lambda length during surgery; (ii) having profuse bleeding during surgery; or (iii) did not survive surgery or died during the experiment. All surviving mice were included in the phenotypic analysis, and we did not eliminate mice because of a missed injection. Immunostaining for mCherry, as described below, was used to validate PVN injection coordinates 8 weeks after injection in several mice with single midline injections showing one side of the PVN to have stronger mCherry expression (Fig. 3C and fig. S10). The majority of mice did not undergo immunostaining as they were used for RNA analyses. Mice were maintained on a picodiet 5058 and weighed on a weekly basis.

Immunostaining

For immunostaining, mice were anesthetized with pentobarbital (7.5 mg/0.15 ml, intraperitoneally) and transcardially perfused with 10 ml of heparinized saline (10 U/ml, 2 ml/min) followed by 10 ml of phosphate-buffered 4% paraformaldehyde (PFA). Brains were removed, postfixed for 24 hours in 4% PFA, and then equilibrated in 30% sucrose in PBS for 72 hours. Brains were coronally sectioned (35 μ m for immunostaining, 50 μ m for stereology) on a sliding microtome (Leica SM 2000R). Immunohistochemistry was performed as previously described (24,57,58). Coronal brain sections that had been stored in PBS at 4°C were permeabilized and blocked in 3% normal goat serum–0.3% Triton X-100

for 1 hour and incubated at 4°C overnight using an antibody to mCherry at a dilution of 1:500 (Abcam ab167453). Sections were placed in 4',6-diamidino-2-phenylindole (DAPI) (0.2 g/ml; 236276; Roche) for 10 min and then mounted on Plus coated slides and coverslipped using Vectashield (H-1000; Vector Laboratories). Images of sections containing PVN were captured on a Zeiss Apotome.

Supplementary Material

Refer to Web version on PubMed Central for supplementary material.

ACKNOWLEDGMENTS

We thank J. Michaud for the *Sim1^{+/-}* mice; M. J. Kim for the SCE2 hypothalamus picture; J. S. Weissman and S. Qi for the dCas9-VP64 plasmids; B. Huang for the *S. aureus* sgRNA vector; C. Paillart for assistance with the metabolic profiling; S. K. Matharu and Y. Ahituv for graphic assistance with the figures; and M. T. McManus, P. Devine, and S. H. Ahanger for helpful discussions.

Funding: This article was supported in part by grant 1R01DK090382 from the National Institute of Diabetes and Digestive and Kidney Diseases (NIDDK), the UCSF Nutrition Obesity Research Center funded by National Institutes of Health grant P30DK098722, and the UCSF School of Pharmacy 2017 Mary Anne Koda-Kimble Seed Award for Innovation. N.A. is also supported by grants by the National Human Genome Research Institute (NHGRI) and Division of Cancer Prevention, National Cancer Institute grant no. 1R01CA197139, National Institute of Mental Health grant no. 1R01MH109907, National Institute of Child and Human Development 1P01HD084387, and NHGRI grant no. 1UM1HG009408. N.M. was supported in part by the UCSF School of Pharmacy 2017 Mary Anne Koda-Kimble Seed Award for Innovation and the UCSF Catalyst Program. S.R. was supported by the Royal Golden Jubilee Ph.D. Program grant no. PHD/007/2554. C.V. is also supported by NIDDK grant nos. R01DK106404 and R01 DK60540-09 and Y.W. by the American Diabetes Association Mentor Based Award-7-12-MN-79. A.H. is supported by the National Institute of General Medical Sciences IRACDA award K12GM081266.

REFERENCES AND NOTES

- Dang VT, Kassahn KS, Marcos AE, Ragan MA, Identification of human haploinsufficient genes and their genomic proximity to segmental duplications. *Eur. J. Hum. Genet* 16, 1350–1357 (2008). doi: 10.1038/ejhg.2008.111; pmid: 18523451 [PubMed: 18523451]
- Landrum MJ et al., ClinVar: Public archive of interpretations of clinically relevant variants. *Nucleic Acids Res.* 44, D862–D868 (2016). doi: 10.1093/nar/gkv1222; pmid: 26582918 [PubMed: 26582918]
- Lek M et al., Analysis of protein-coding genetic variation in 60,706 humans. *Nature* 536, 285–291 (2016). doi: 10.1038/nature19057; pmid: 27535533 [PubMed: 27535533]
- Bender E, Gene therapy: Industrial strength. *Nature* 537, S57–S59 (2016). doi: 10.1038/537S57a; pmid: 27602741 [PubMed: 27602741]
- Kotterman MA, Schaffer DV, Engineering adeno-associated viruses for clinical gene therapy. *Nat. Rev. Genet.* 15, 445–451 (2014). doi: 10.1038/nrg3742; pmid: 24840552 [PubMed: 24840552]
- Samulski RJ, Muzyczka N, AAV-mediated gene therapy for research and therapeutic purposes. *Annu. Rev. Virol.* 1, 427–451 (2014). doi: 10.1146/annurev-virology-031413-085355; pmid: 26958729 [PubMed: 26958729]
- Lykken EA, Shyng C, Edwards RJ, Rozenberg A, Gray SJ, Recent progress and considerations for AAV gene therapies targeting the central nervous system. *J. Neurodev. Disord.* 10, 16 (2018). doi: 10.1186/s11689-018-9234-0; pmid: 29776328 [PubMed: 29776328]
- Wu Z, Yang H, Colosi P, Effect of genome size on AAV vector packaging. *Mol. Ther.* 18, 80–86 (2010). doi: 10.1038/mt.2009.255; pmid: 19904234 [PubMed: 19904234]
- Gilbert LA et al., CRISPR-mediated modular RNA-guided regulation of transcription in eukaryotes. *Cell* 154, 442–451 (2013). doi: 10.1016/j.cell.2013.06.044; pmid: 23849981 [PubMed: 23849981]

10. Perez-Pinera P et al., RNA-guided gene activation by CRISPR-Cas9-based transcription factors. *Nat. Methods* 10, 973–976 (2013). doi: 10.1038/nmeth.2600; pmid: 23892895 [PubMed: 23892895]
11. Konermann S et al., Genome-scale transcriptional activation by an engineered CRISPR-Cas9 complex. *Nature* 517, 583–588 (2015) pmid: 25494202 [PubMed: 25494202]
12. Hilton IB et al., Epigenome editing by a CRISPR-Cas9-based acetyltransferase activates genes from promoters and enhancers. *Nat. Biotechnol.* 33, 510–517 (2015). doi: 10.1038/nbt.3199; pmid: 25849900 [PubMed: 25849900]
13. Chavez A et al., Highly efficient Cas9-mediated transcriptional programming. *Nat. Methods* 12, 326–328 (2015). doi: 10.1038/nmeth.3312; pmid: 25730490 [PubMed: 25730490]
14. Maeder ML et al., CRISPR RNA-guided activation of endogenous human genes. *Nat. Methods* 10, 977–979 (2013). doi: 10.1038/nmeth.2598; pmid: 23892898 [PubMed: 23892898]
15. Kiani S et al., Cas9 gRNA engineering for genome editing, activation and repression. *Nat. Methods* 12, 1051–1054 (2015). doi: 10.1038/nmeth.3580; pmid: 26344044 [PubMed: 26344044]
16. Michaud JL, Rosenquist T, May NR, Fan CM, Development of neuroendocrine lineages requires the bHLH-PAS transcription factor SIM1. *Genes Dev.* 12, 3264–3275 (1998). doi: 10.1101/gad.12.20.3264; pmid: 9784500 [PubMed: 9784500]
17. Beckers S, Zegers D, Van Gaal LF, Van Hul W, The role of the leptin-melanocortin signalling pathway in the control of food intake. *Crit. Rev. Eukaryot. Gene Expr.* 19, 267–287 (2009). doi: 10.1615/CritRevEukarGeneExpr.v19.i4.20; pmid: 19817705 [PubMed: 19817705]
18. Holder JL Jr., Butte NF, Zinn AR, Profound obesity associated with a balanced translocation that disrupts the SIM1 gene. *Hum. Mol. Genet* 9, 101–108 (2000). doi: 10.1093/hmg/9.1.101; pmid: 10587584 [PubMed: 10587584]
19. Ahituv N et al., Medical sequencing at the extremes of human body mass. *Am. J. Hum. Genet.* 80, 779–791 (2007). doi: 10.1086/513471; pmid: 17357083 [PubMed: 17357083]
20. Ramachandrapa S et al., Rare variants in single-minded 1 (SIM1) are associated with severe obesity. *J. Clin. Invest.* 123, 3042–3050 (2013). doi: 10.1172/JCI68016; pmid: 23778139 [PubMed: 23778139]
21. Bonnefond A et al., Loss-of-function mutations in SIM1 contribute to obesity and Prader-Willi-like features. *J. Clin. Invest.* 123, 3037–3041 (2013). doi: 10.1172/JCI68035; pmid: 23778136 [PubMed: 23778136]
22. Michaud JL et al., Sim1 haploinsufficiency causes hyperphagia, obesity and reduction of the paraventricular nucleus of the hypothalamus. *Hum. Mol. Genet.* 10, 1465–1473 (2001). doi: 10.1093/hmg/10.14.1465; pmid: 11448938 [PubMed: 11448938]
23. Tolson KP et al., Postnatal Sim1 deficiency causes hyperphagic obesity and reduced Mc4r and oxytocin expression. *J. Neurosci.* 30, 3803–3812 (2010). doi: 10.1523/JNEUROSCI.5444-09.2010; pmid: 20220015 [PubMed: 20220015]
24. Kublaoui BM, Holder JL Jr., Tolson KP, Gemelli T, Zinn AR, SIM1 overexpression partially rescues agouti yellow and diet-induced obesity by normalizing food intake. *Endocrinology* 147, 4542–4549 (2006). doi: 10.1210/en.2006-0453; pmid: 16709610 [PubMed: 16709610]
25. Krashes MJ, Lowell BB, Garfield AS, Melanocortin-4 receptor-regulated energy homeostasis. *Nat. Neurosci.* 19, 206–219 (2016). doi: 10.1038/nn.4202; pmid: 26814590 [PubMed: 26814590]
26. Lubrano-Berthelier C et al., Melanocortin 4 receptor mutations in a large cohort of severely obese adults: Prevalence, functional classification, genotype-phenotype relationship, and lack of association with binge eating. *J. Clin. Endocrinol. Metab.* 91, 1811–1818 (2006). doi: 10.1210/jc.2005-1411; pmid: 16507637 [PubMed: 16507637]
27. Vaisse C et al., Melanocortin-4 receptor mutations are a frequent and heterogeneous cause of morbid obesity. *J. Clin. Invest.* 106, 253–262 (2000). doi: 10.1172/JCI9238; pmid: 10903341 [PubMed: 10903341]
28. Farooqi IS et al., Clinical spectrum of obesity and mutations in the melanocortin 4 receptor gene. *N. Engl. J. Med.* 348, 1085–1095 (2003). doi: 10.1056/NEJMoa022050; pmid: 12646665 [PubMed: 12646665]
29. Huszar D et al., Targeted disruption of the melanocortin-4 receptor results in obesity in mice. *Cell* 88, 131–141 (1997). doi: 10.1016/S0092-8674(00)81865-6; pmid: 9019399 [PubMed: 9019399]

30. Yang C, Boucher F, Tremblay A, Michaud JL, Regulatory interaction between arylhydrocarbon receptor and SIM1, two basic helix-loop-helix PAS proteins involved in the control of food intake. *J. Biol. Chem.* 279, 9306–9312 (2004). doi: 10.1074/jbc.M307927200; pmid: 14660629 [PubMed: 14660629]
31. Kim MJ, Oksenberg N, Hoffmann TJ, Vaisse C, Ahituv N, Functional characterization of SIM1-associated enhancers. *Hum. Mol. Genet* 23, 1700–1708 (2014). pmid: 24203700 [PubMed: 24203700]
32. Flint J, Shenk T, Viral transactivating proteins. *Annu. Rev Genet* 31,177–212 (1997). doi: 10.1146/annurev.genet.31.1.177; pmid: 9442894 [PubMed: 9442894]
33. Chavez A et al., Comparison of Cas9 activators in multiple species. *Nat. Methods* 13, 563–567 (2016). doi: 10.1038/nmeth.3871; pmid: 27214048 [PubMed: 27214048]
34. Tasic B et al., Site-specific integrase-mediated transgenesis in mice via pronuclear injection. *Proc. Natl. Acad. Sci. U.S.A.* 108, 7902–7907 (2011). doi: 10.1073/pnas.1019507108; pmid: 21464299 [PubMed: 21464299]
35. Hippenmeyer S et al., Genetic mosaic dissection of *Lis1* and *Ndel1* in neuronal migration. *Neuron* 68, 695–709 (2010). doi: 10.1016/j.neuron.2010.09.027; pmid: 21092859 [PubMed: 21092859]
36. Su AI et al., A gene atlas of the mouse and human proteinencoding transcriptomes. *Proc. Natl. Acad. Sci. U.S.A.* 101, 6062–6067 (2004). doi: 10.1073/pnas.0400782101; pmid: 15075390 [PubMed: 15075390]
37. Petryszak R et al., Expression Atlas update—An integrated database of gene and protein expression in humans, animals and plants. *Nucleic Acids Res.* 44 (D1), D746–D752 (2016). doi: 10.1093/nar/gkv1045; pmid: 26481351 [PubMed: 26481351]
38. Bae S, Park J, Kim JS, Cas-OFFinder: A fast and versatile algorithm that searches for potential off-target sites of Cas9 RNA-guided endonucleases. *Bioinformatics* 30, 1473–1475 (2014). doi: 10.1093/bioinformatics/btu048; pmid: 24463181 [PubMed: 24463181]
39. Zincarelli C, Soltys S, Rengo G, Rabinowitz JE, Analysis of AAV serotypes 1–9 mediated gene expression and tropism in mice after systemic injection. *Mol. Ther.* 16, 1073–1080 (2008). doi: 10.1038/mt.2008.76; pmid: 18414476 [PubMed: 18414476]
40. Weise A et al., Microdeletion and microduplication syndromes. *J. Histochem. Cytochem.* 60, 346–358 (2012). doi: 10.1369/0022155412440001; pmid: 22396478 [PubMed: 22396478]
41. Horlbeck MA et al., Nucleosomes impede Cas9 access to DNA in vivo and in vitro. *eLife* 5, e12677 (2016). doi: 10.7554/eLife.12677; pmid: 26987018
42. Simeonov DR et al., Discovery of stimulation-responsive immune enhancers with CRISPR activation. *Nature* 549, 111–115 (2017). doi: 10.1038/nature23875; pmid: 28854172 [PubMed: 28854172]
43. Otchy TM et al., Acute off-target effects of neural circuit manipulations. *Nature* 528, 358–363 (2015). doi: 10.1038/nature16442; pmid: 26649821 [PubMed: 26649821]
44. Gongalves JPL, Palmer D, Meldal M, MC4R Agonists: Structural overview on antiobesity therapeutics. *Trends Pharmacol. Sci.* 39, 402–423 (2018). pmid: 29478721 [PubMed: 29478721]
45. Collet TH et al., Evaluation of a melanocortin-4 receptor (MC4R) agonist (Setmelanotide) in MC4R deficiency. *Mol. Metab.* 6, 1321–1329 (2017). doi: 10.1016/j.molmet.2017.06.015; pmid: 29031731 [PubMed: 29031731]
46. Ran FA et al., In vivo genome editing using *Staphylococcus aureus* Cas9. *Nature* 520, 186–191 (2015). doi: 10.1038/nature14299; pmid: 25830891 [PubMed: 25830891]
47. Deng W et al., Reactivation of developmentally silenced globin genes by forced chromatin looping. *Cell* 158, 849–860 (2014). doi: 10.1016/j.cell.2014.05.050; pmid: 25126789 [PubMed: 25126789]
48. Canver MC et al., BCL11A enhancer dissection by Cas9-mediated in situ saturating mutagenesis. *Nature* 527, 192–197 (2015). doi: 10.1038/nature15521; pmid: 26375006 [PubMed: 26375006]
49. Hirst RC, McCullagh KJ, Davies KE, Utrophin upregulation in Duchenne muscular dystrophy. *Acta Myol.* 24, 209–216 (2005). pmid: 16629055 [PubMed: 16629055]
50. Liao HK et al., In vivo target gene activation via CRISPR/Cas9-mediated trans-epigenetic modulation. *Cell* 171, 1495–1507.e15 (2017). doi: 10.1016/j.cell.2017.10.025; pmid: 29224783 [PubMed: 29224783]

51. Sproule DM, Kaufmann P, Therapeutic developments in spinal muscular atrophy. *Ther. Adv. Neurol. Disorder.* 3, 173–185 (2010). doi: 10.1177/1756285610369026; pmid: 21179609
52. Dobin A et al., STAR: Ultrafast universal RNA-seq aligner. *Bioinformatics* 29, 15–21 (2013). doi: 10.1093/bioinformatics/bts635; pmid: 23104886 [PubMed: 23104886]
53. Love MI, Huber W, Anders S, Moderated estimation of fold change and dispersion for RNA-seq data with DESeq2. *Genome Biol.* 15, 550 (2014). doi: 10.1186/s13059-014-0550-8; pmid: 25516281 [PubMed: 25516281]
54. Zhang Y et al., Model-based analysis of ChIP-Seq (MACS). *Genome Biol.* 9, R137 (2008). doi: 10.1186/gb-2008-9-9-r137; pmid: 18798982 [PubMed: 18798982]
55. Nagy A, Gertsenstein M, Vintersten K, Behringer R, *Manipulating the Mouse Embryo: A Laboratory Manual* (Cold Spring Harbor, New York, ed. 3, 2002).
56. Siljee JE et al., Subcellular localization of MC4R with ADCY3 at neuronal primary cilia underlies a common pathway for genetic predisposition to obesity. *Nat. Genet.* 50, 180–185 (2018). doi: 10.1038/s41588-017-0020-9; pmid: 29311635 [PubMed: 29311635]
57. Beuckmann CT et al., Expression of a poly-glutamine-ataxin-3 transgene in orexin neurons induces narcolepsy-cataplexy in the rat. *J. Neurosci.* 24, 4469–4477 (2004). doi: 10.1523/JNEUROSCI.5560-03.2004; pmid: 15128861 [PubMed: 15128861]
58. Kublaoui BM, Gemelli T, Tolson KP, Wang Y, Zinn AR, Oxytocin deficiency mediates hyperphagic obesity of Sim1 haploinsufficient mice. *Mol. Endocrinol.* 22, 1723–1734 (2008). doi: 10.1210/me.2008-0067; pmid: 18451093 [PubMed: 18451093]

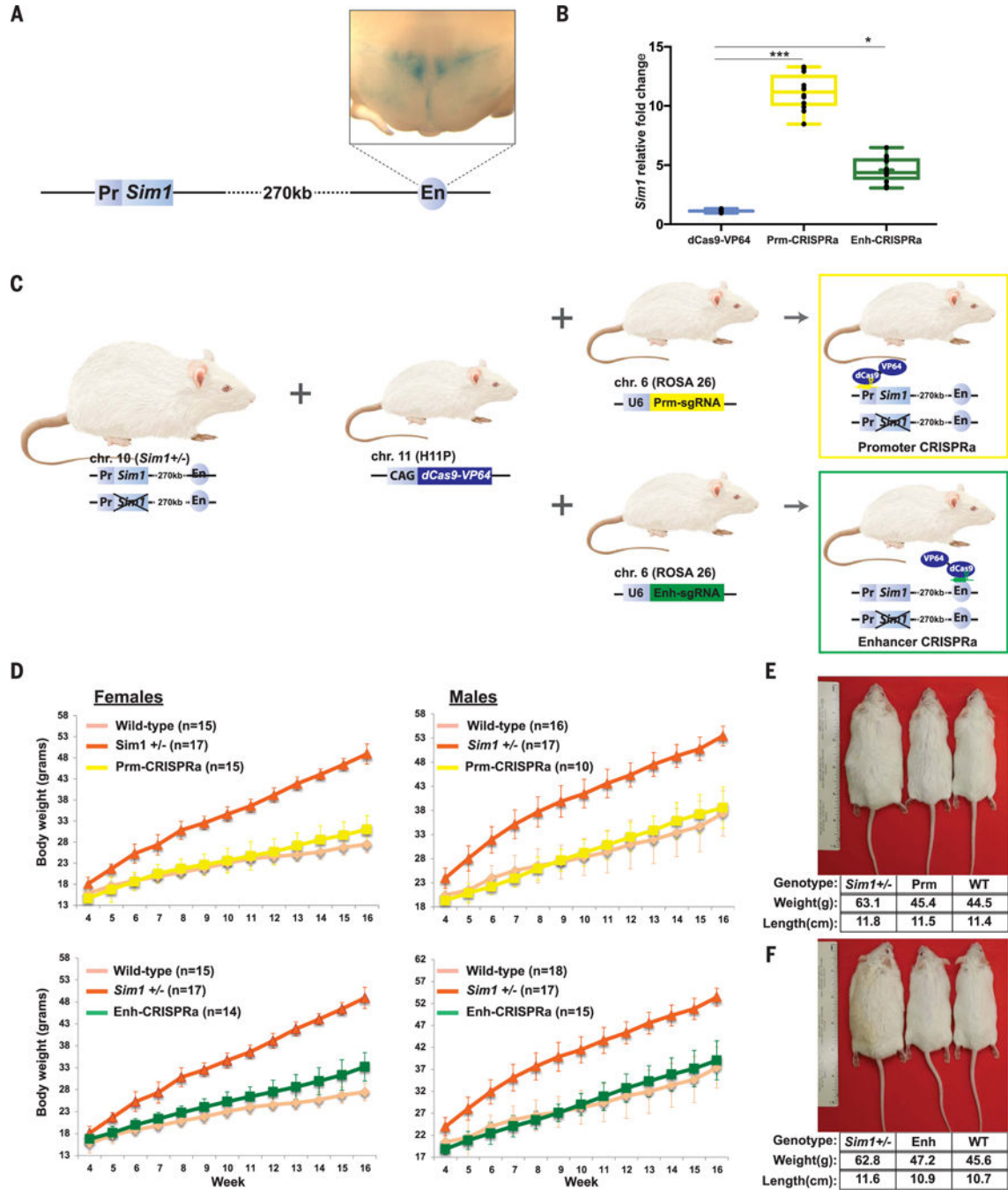


Fig. 1. CRISPRa *Sim1* up-regulation in vitro and obesity rescue in vivo. (A) Schema of the mouse *Sim1* genomic locus, showing the LacZ-driven hypothalamic expression of SCE2 (En) from 56-day-old mice. (B) CRISPRa in Neuro-2a cells targeting the *Sim1* promoter (Prm-CRISPRa) or enhancer (Enh-CRISPRa). Results are expressed as mRNA fold increase normalized to *Actb* using the $\Delta\Delta C_T$ method. The data are represented as means \pm the lower and upper quartile, and lines represent the minimum and maximum from three independent experiments and three technical replicates. * $p < 0.001$; *** $p < 0.0005$ (ANOVA, Tukey test). (C) Schema showing the mating scheme used to generate

Sim1^{+/-} CRISPRa mice. A CAG-dCas9-VP64 cassette was knocked into the *Hipp11* (H11P3) locus, and an sgRNA targeting either the *Sim1* promoter (U6-Prm-sgRNA) or SCE2 (U6-Enh-sgRNA) was knocked into the *Rosa26* locus. **(D)** Weekly weight measurements of wild-type, *Sim1*^{+/-}, *H11P3*^{CAG-dCas9-VP64} × *R26P3*^{Sim1Pr-sgRNA} (Prm-CRISPRa), and *H11P3*^{CAG-dCas9-VP64} × *R26P3*^{SCE2En-sgRNA} (Enh-CRISPRa). At least 10 male and female mice were measured per genotype. Mean values ± SD are shown. *p*-value statistics are listed in table S5. **(E and F)** Photos of 26-week-old male mice for each genotype: *Sim1*^{+/-}, *H11P3*^{CAG-dCas9-VP64} × *R26P3*^{Sim1Pr-sgRNA} (Prm), and wild type (WT) (E) and *Sim1*^{+/-}, *H11P3*^{CAG-dCas9-VP64} × *R26P3*^{SCE2En-sgRNA} (Enh), and wild type (WT) (F). Genotype, weight, and length of each mouse are depicted below.

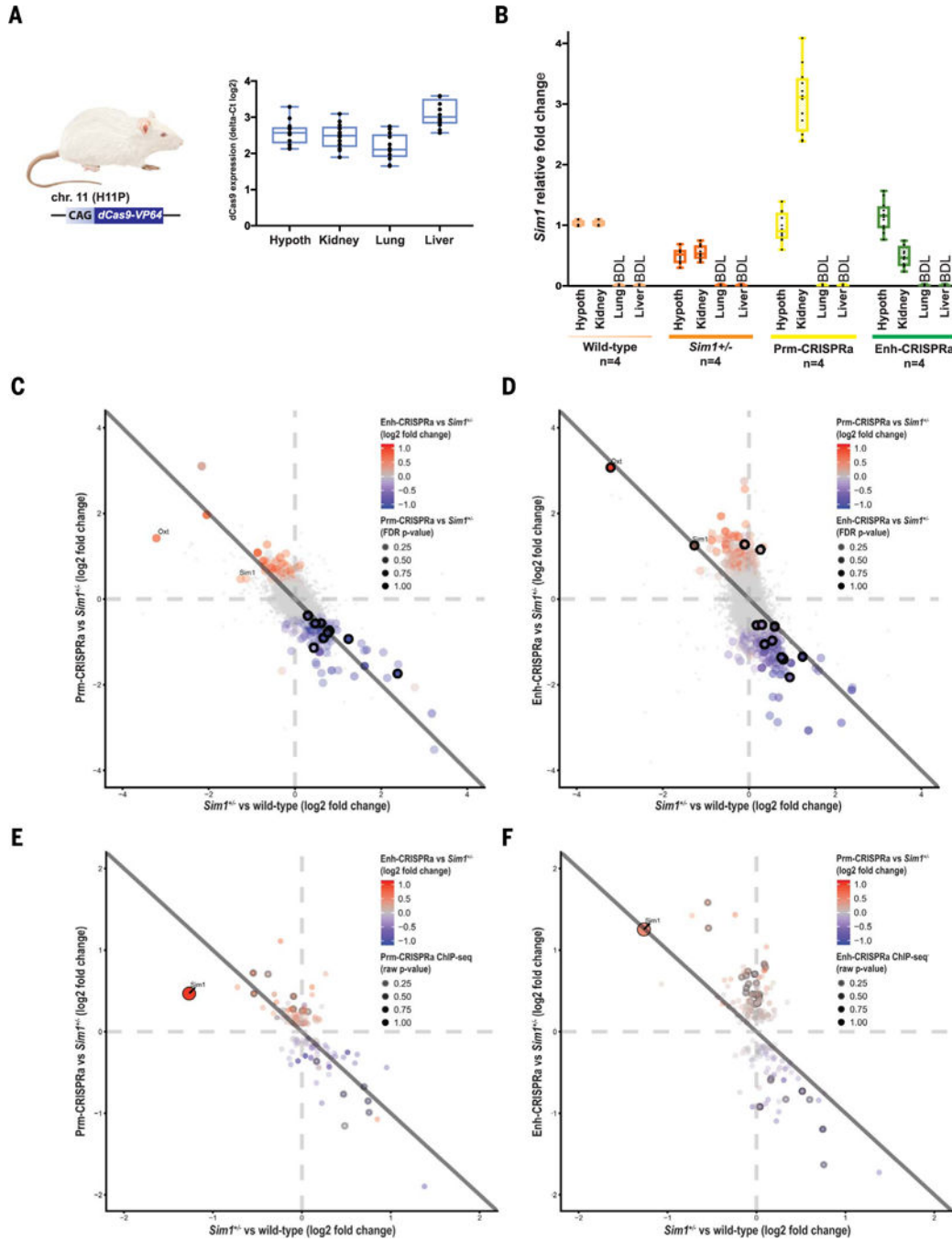


Fig. 2. *dCas9* and *Sim1* mRNA expression levels in CRISPRa transgenic mice.

(A) *dCas9* mRNA expression in the hypothalamus, kidney, lung, and liver from four *Sim1*^{+/-} × *H11P3*^{CAG-dCas9-VP64} mice. The data are represented as means ± the lower and upper quartile, and lines represent the minimum and maximum from at least four mice with three technical replicates. (B) *Sim1* mRNA expression in the hypothalamus, kidney, lung, and liver for the following genotypes: wild type, *Sim1*^{+/-}, *H11P3*^{CAG-dCas9-VP64} × *R26P3*^{Sim1Pr-sgRNA} (Prm-CRISPRa), and *H11P3*^{CAG-dCas9-VP64} × *R26P3*^{SCE2En-sgRNA} (Enh-CRISPRa). The data are represented as means ± the lower and upper quartile, and lines

represent the minimum and maximum from four mice (two females and two males) and three technical replicates. All experiments were determined based on mRNA fold increase compared to wild type and normalized to *Actb* or *Rpl38* using the $\Delta\Delta CT$ method or ΔCT for (A). BDL, below detectable levels. (C and D) A Michaelis-Menten plot showing differentially expressed genes in the hypothalamus between *Sim1*^{+/-} and wild-type mice on the *x* axis and Prm-CRISPRa (C) or Enh-CRISPRa (D) versus *Sim1*^{+/-} mice on the *y* axis. The larger circles are genes that are differentially expressed with a raw *p* value ≤ 0.05 , and the outlined circles have a FDR ≤ 0.1 . (E and F) A Michaelis-Menten plot showing differentially expressed genes in the hypothalamus that are nearby ChIP-seq peaks and predicted off-target sgRNAs between *Sim1*^{+/-} and wild-type mice on the *x* axis and Prm-CRISPRa (E) or Enh-CRISPRa (F) versus *Sim1*^{+/-} mice on the *y* axis. The outlined circles are genes that show differential expression with a raw *p* value ≤ 0.05 , and the larger circles are genes that overlap nearby off-target sites (both *Sim1* promoter and SCE2 were predicted targets even up to three mismatches).

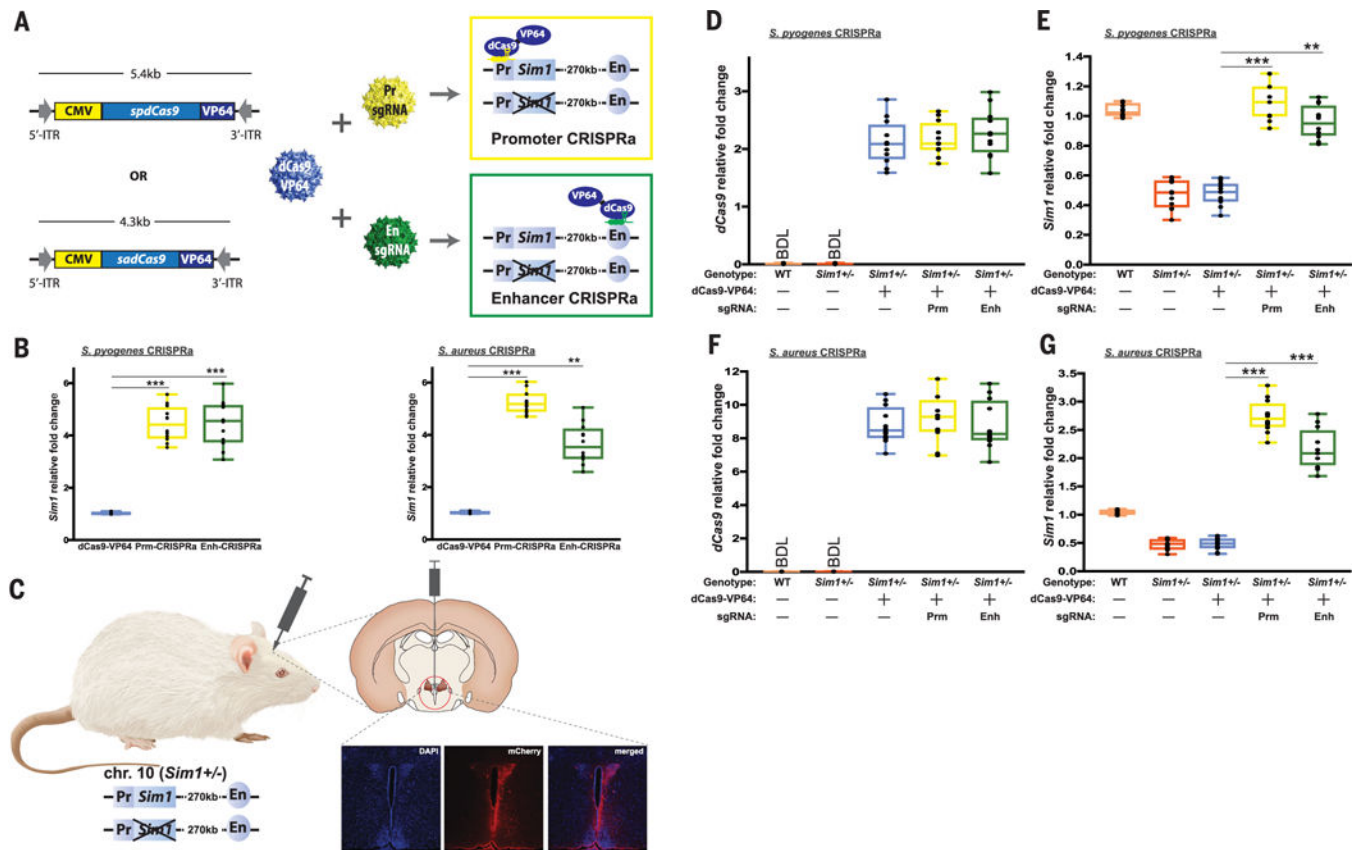


Fig. 3. CRISPRa *Sim1* overexpression in vitro and in vivo by using AAV.

(A) Schema showing the various *S. pyogenes* and *S. aureus* AAVs used for *Sim1* CRISPRa.

(B) *S. pyogenes* (left) and *S. aureus* (right) AAV CRISPRa in Neuro-2a cells using virions containing *pCMV-dCas9-VP64* (dCas9-VP64), *pCMV-dCas9-VP64* along with *pSim1Pr-mCherry* (Prm-CRISPRa), and *pCMV-dCas9-VP64* along with *pSCE2En-mCherry* (Enh-CRISPRa). Results are expressed as mRNA fold increase normalized to *Actb* using the

CT method. The data are represented as means \pm the lower and upper quartile, and lines represent the minimum and maximum from four independent experiments with three technical replicates. *** $p < 0.0005$; ** $p < 0.001$ (ANOVA, Tukey test). (C) Schema showing location of the single midline stereotaxic injection in the PVN (red circle) followed by immunohistochemistry results from *pSim1Pr-mCherry*-injected hypothalami of 12-week-old mice showing DAPI (4',6-diamidino-2-phenylindole) staining, mCherry expression, and merged staining of both. (D and E) *dCas9* (D) and *Sim1* (E) mRNA expression from noninjected wild-type and *Sim1*^{+/-} mice along with *pCMV-spdCas9-VP64* (dCas9-VP64)-, *pCMV-spdCas9-VP64* + *pSim1Pr-mCherry* (Prm-CRISPRa)-, and *pCMV-spdCas9-VP64* + *pSCE2En-mCherry* (Enh-CRISPRa)-injected *Sim1*^{+/-} mice for *S. pyogenes*. (F and G) *dCas9* (F) and *Sim1* (G) mRNA expression from noninjected wild-type and *Sim1*^{+/-} mice along with *pCMV-sadCas9-VP64* (dCas9-VP64)-, *pCMV-sadCas9-VP64* + *pSim1Pr-mCherry* (Prm-CRISPRa)-, and *pCMV-sadCas9-VP64* + *pSCE2En-mCherry* (Enh-CRISPRa)-injected *Sim1*^{+/-} mice for *S. aureus*. Four mice were used for each genotype. The data are represented as means \pm the lower and upper quartile, and lines represent the minimum and maximum. Values from four independent experiments with three technical

replicates were determined based on mRNA fold increase compared to wild-type mice and normalized to *Actb* using the $\Delta\Delta$ CT method for *Sim1* expression and relative *Actb* $\Delta\Delta$ CT log2 for *dCas9* expression.

Author Manuscript

Author Manuscript

Author Manuscript

Author Manuscript

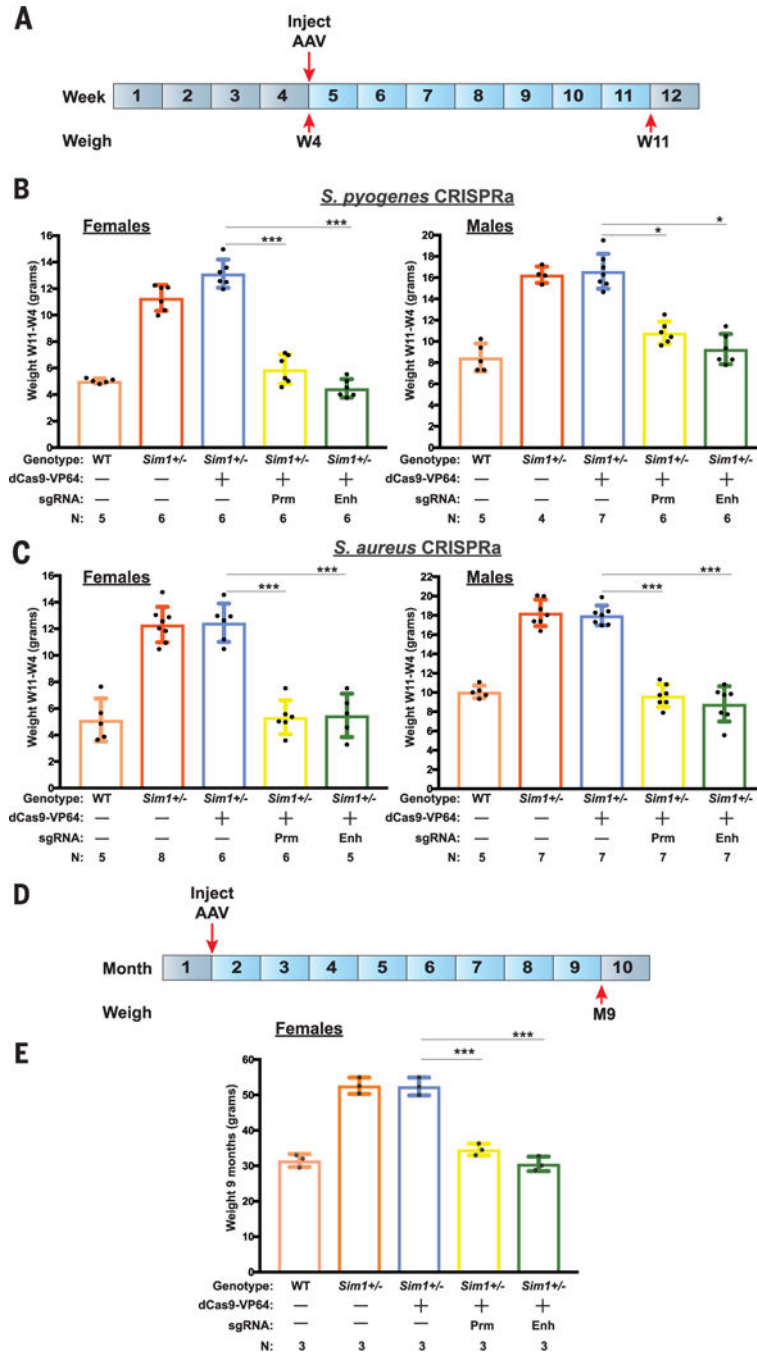


Fig. 4. CRISPRa-AAV injection in the PVN decreases weight gain in *Sim1*^{+/-} mice. (A) Timeline for weight measurement after CRISPRa-AAV injection in PVN. (B and C) Weight gain determined over a 7-week period from *Sim1*^{+/-} mice injected with *pCMV-dCas9-VP64* (dCas9-VP64), *pCMV-dCas9-VP64 + pSim1Pr-mCherry* (Prm-CRISPRa), or *pCMV-dCas9-VP64 + pSCE2En-mCherry* (Enh-CRISPRa) compared to uninjected wild-type littermates and *Sim1*^{+/-} mice using *S. pyogenes* (B) or *S. aureus* (C) CRISPRa. Means \pm SD and number of mice (N) are shown per condition. * $p < 0.001$; *** $p < 0.0005$; n.s., not significant (ANOVA, Tukey test). (D) Monthly timeline for weight measurement after

CRISPRa-AAV injection in PVN. (E) dCas9-VP64, Prm-CRISPRa, and Enh-CRISPRa compared to uninjected wild-type littermates and *Sim1*^{+/-} mice 9 months after injection. Means \pm SD and number of mice (*N*) are shown per condition. ****p* < 0.0005.

Author Manuscript

Author Manuscript

Author Manuscript

Author Manuscript

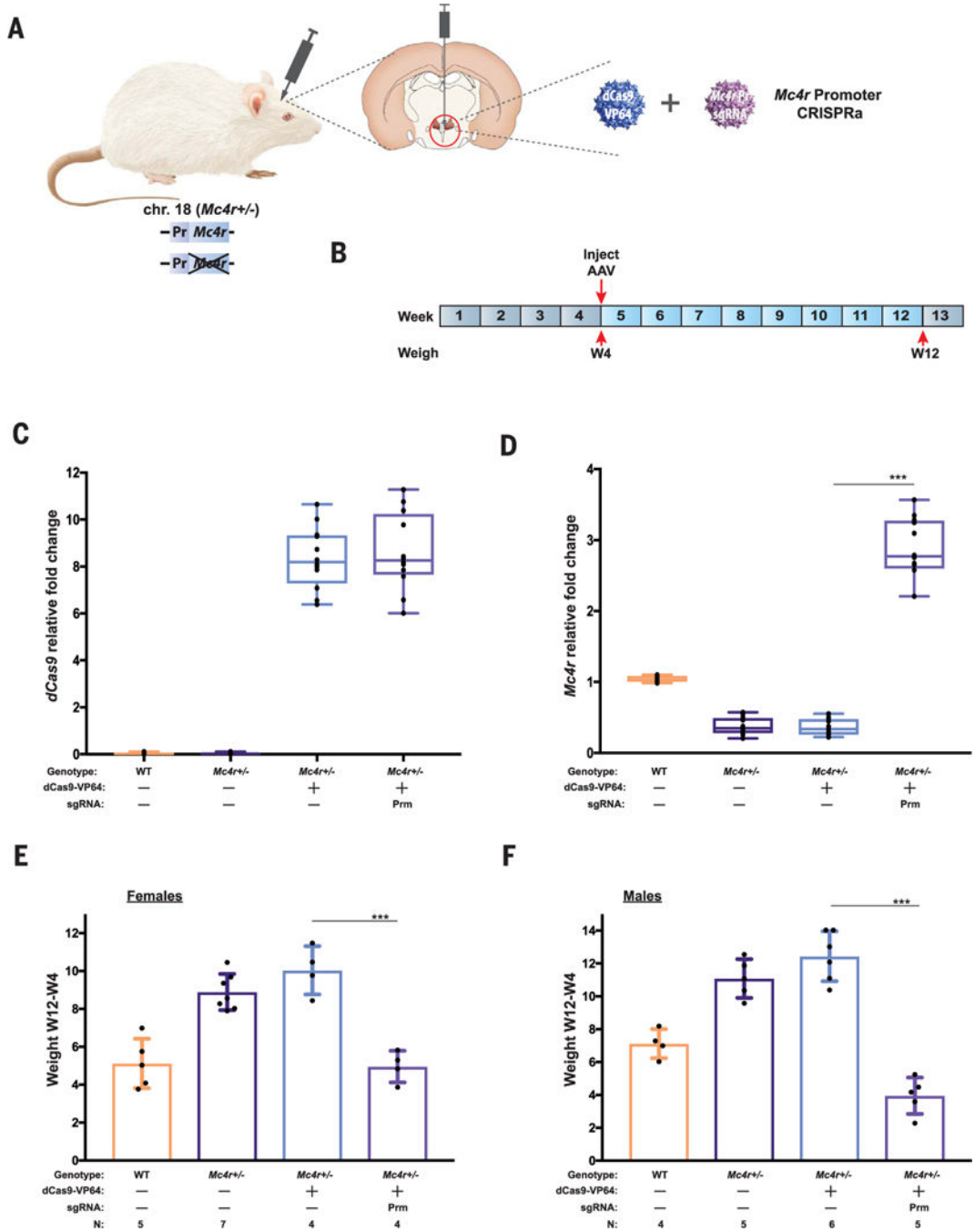


Fig. 5. CRISPRa-AAV injection in the PVN decreases weight gain in *Mc4r*^{+/-} mice. (A) Schema showing the CRISPR AAVs used for injection into *Mc4r*^{+/-} mice. (B) Timeline for weight measurement post CRISPRa-AAV injection in PVN. (C and D) *dCas9* (C) and *Mc4r* (D) mRNA expression from uninjected wild-type and *Mc4r*^{+/-} mice along with *pCMV-sadCas9-VP64* (*dCas9*-VP64)- and *pCMV-sadCas9-VP64 + pMc4rPr-mCherry* (Prm-CRISPRa)-injected *Mc4r*^{+/-} mice. Four mice were used for each genotype with three technical replicates. The data are represented as means ± the lower and upper quartile, and lines represent the minimum and maximum. Values were determined based on mRNA fold

increase compared to wild-type mice and normalized to *Actb* using the $\Delta\Delta$ CT method for *Mc4r* expression and relative *Actb* Δ CT log2 for *dCas9* expression. (E and F) Weight gain determined over an 8-week period from *Mc4r*^{+/-} female (E) or male (F) mice injected with *pCMV-sadCas9-VP64* (dCas9-VP64) or *pCMV-sadCas9-VP64 + pMc4rPr-mCherry* (Prm-CRISPRa) compared to uninjected wild-type littermates and *Mc4r*^{+/-} mice. Means \pm SD and number of mice (*N*) are shown for each condition. ****p* < 0.0005; (ANOVA, Tukey test).

Author Manuscript

Author Manuscript

Author Manuscript

Author Manuscript

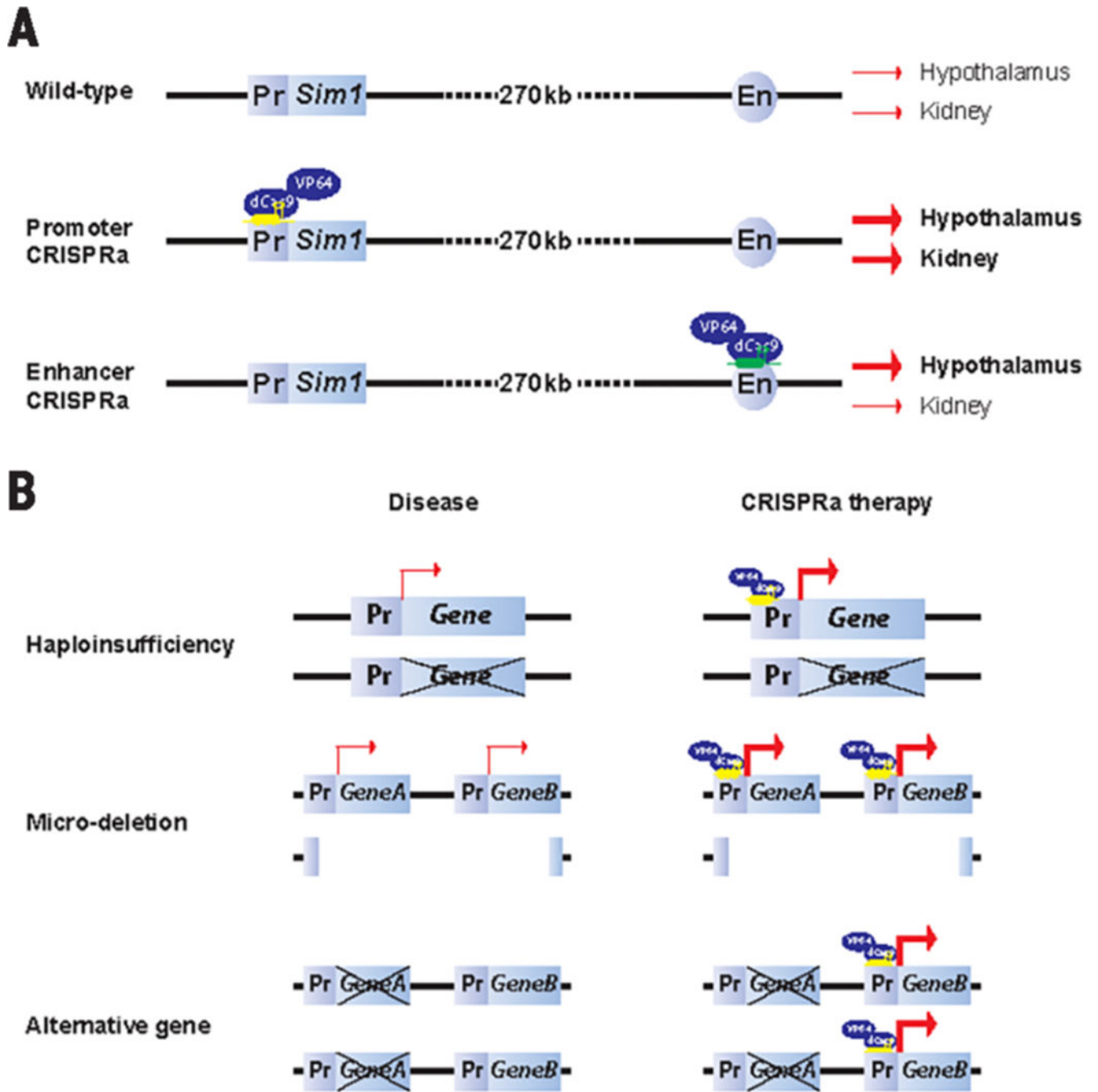


Fig. 6. CRISPRa potential therapeutic strategy. (A) Tissue-specific differences in gene activation due to the type of targeted cis-regulatory element (promoter or enhancer). (B) CRISPRa can be used as a tool to rescue haploinsufficiency by up-regulating the expression of the endogenous functional allele. It can also be used to up-regulate a gene or genes that are deleted in microdeletions or an alternate gene with a function similar to that of the disease-mutated gene.